THE JOURNAL OF PHYSICAL CHEMISTRY C
A JOURNAL OF THE AMERICAN CHEMICAL SOCIETY

pubs.acs.org/JPCC
Article

Origin of Macroscopic Observables of Strongly Coupled Metal Nanoparticle−Molecule Systems from Microscopic Electronic Properties

Maria Bancerek, Jakub Fojt, Paul Erhart, and Tomasz J. Antosiewicz*

Cite This: https://doi.org/10.1021/acs.jpcc.4c02200
Read Online

ABSTRACT: Strongly coupled light−matter systems are becoming a ubiquitous platform for investigating an increasing number of physical phenomena from modifying charge transport, altered emission, and relaxation pathways to selective or enhanced chemical reactivity. Such systems are investigated across a large length scale from few-nanometer-sized particles to macroscopic cavities encompassing many interacting moieties. Describing these numerous and varied physical systems is attempted in various ways from classical coupled harmonic oscillator models through quantum Hamiltonians to ab initio modeling. Here, by combining time-dependent density functional theory modeling and analysis with macroscopic models, we elucidate the origin of modifications of effective interaction parameters in terms of microscopic changes to the electronic density and Kohn−Sham transitions of the plasmonic particle and its coupled molecular counterpart. Specifically, we demonstrate how the emergence of mixed metal-molecular states and transitions modifies the effective resonances of the underlying plasmon and molecule in the regime of strong coupling and how these changes subsequently lead to the formation of mixed light−matter polaritons.

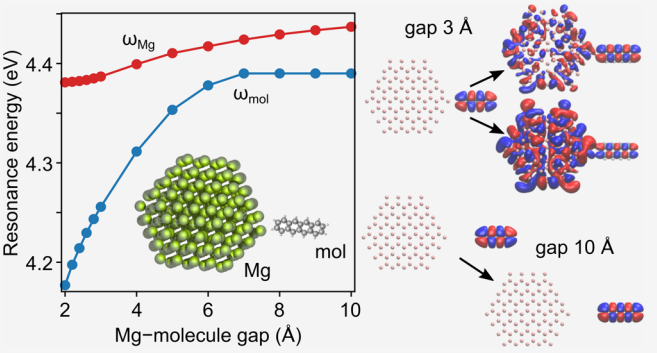

INTRODUCTION

Strong coupling between light and matter has received a lot of interest in the last years due to the prospects for modifying physicochemical properties of such strongly coupled systems.[1−3] When the energy exchange rate between photonic modes and optical transitions exceeds the losses in the system, the strong light−matter coupling regime is achieved, and the emergent hybrid light−matter states, polaritons, form. These can give rise to modified properties such as altered solvent polarity[4] or chemical reactivity,[5] enhanced conductivity[6,7] or modified emission/relaxation pathways,[8−10] to name a few.

One of the simpler systems capable of reaching the strong coupling regime are plasmonic-molecular assemblies.[1,3] When resonantly excited, plasmonic nanoparticles (NPs) support collective oscillations of conduction electrons in the material, giving rise to the so-called localized surface plasmon resonance (LSPR). The LSPR energy depends on the shape of the NP and can be red-shifted by enlarging its corresponding dimension.[11] At the LSPR, the electric field is greatly enhanced in the vicinity of the NP, i.e., such resonators can serve as tunable optical cavities, confining light to small volumes.[12] Such confined and enhanced electric fields[13] greatly enhance rates of processes occurring in those volumes. If an emitter, e.g., a molecule or a quantum dot, tuned to the resonance energy of the cavity, is added to such a plasmonic system, the strong light−matter interaction regime can be reached.[14,15]

Focusing on plasmonic systems, strong coupling has been observed for ensembles of emitters[15−18] as well as for single emitters[19−21] coupled to various types of modes supported by metal nanostructures. Recent theoretical studies show how strong light−matter coupling can be achieved already at the single molecule level[22,23] and how such relatively small systems consisting of a few hundred atoms can be tackled by first-principles methods, such as density functional theory (DFT)/time-dependent density functional theory (TDDFT). Full electronic TDDFT calculations enable capture of atomistic scale effects and interactions between various electronic states, bright or dark, which are crucial to understand the modifications of the coupled system. Furthermore, ab initio approaches are presently being augmented, e.g., by quantum electrodynamics[24] or via a discrete interaction model/quantum

Received: April 3, 2024
Revised: May 22, 2024
Accepted: May 24, 2024

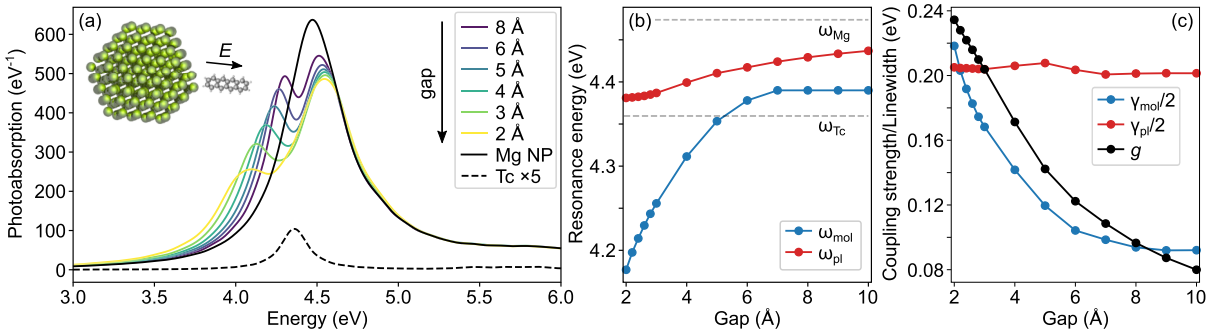

Figure 1. (a) Photoabsorption spectra of the studied system for various gaps between nanoparticle (NP) and tetracene (Tc). The reference spectra of the isolated NP and molecule are plotted with black lines. The inset shows the NP−molecule complex. (b, c) Parameters obtained by fitting the coupled oscillator model, eq 3, to photoabsorption spectra. The gray dashed lines in (b) mark the resonance energies of the isolated NP and molecule.

mechanical method,[25] to bridge the length scale differences inherent in modeling interactions between molecules and light in macroscopic cavities. Hence, these endeavors pave the way for studying the fundamental plasmon-exciton coupling mechanisms.

An interesting avenue of research is the excited state dynamics and energy transfer processes between metal NPs and adsorbed molecules under various conditions.[26−28] In this context, the strong coupling regime is especially promising, since the initial eigenstates become thoroughly mixed, which leads to the formation of new energy states and potentially favorable electron transition possibilities.[29] These changes of the electronic landscape yield modifications of reaction pathways,[30−33] allowing for modified chemistry,[24] catalytic applications,[34] or enhanced selectivity.[35] When two moieties are placed in close proximity and are energetically tuned to each other's transitions, as is the case in the strong coupling regime, resonance energy transfer occurs,[36] which can aid in the extraction of hot carriers generated during plasmon decay in plasmonic-molecular systems.[37,38] This macroscale coupling thus becomes an important tool in tailoring excited-state properties, such as hot carrier transfer across metal−semiconductor interfaces[26,39] or to an adsorbed molecule.[40,41] Polariton modification of energy transport is also observed at lower energies in the vibrational regime by coupling molecules to macroscopic Fabry−Perot cavities. This is enabled by the additional photonic degrees of freedom which mediate interactions between molecules, leading to additional electron−electron correlations over large distances.[42] The result of such modifications is altered, distance-independent charge-transfer properties with selectively improved efficiency. Numerous modeling efforts have gone into unraveling the interplay between the light and electronic/vibrational modes to propose rational design approaches for cavity-molecule systems to realize coherent exciton transport,[43] modify chemical reactions,[44] or tune triplet electroluminescence.[45] It is thus rather clear that modification of the energy landscape and delocalization of the wave functions formed by strong coupling to a specifically designed photonic environment can facilitate and enable tailoring of energy transfer processes, opening possibilities for a new class of nanoscale devices.

METHODS: MODELING NANOSCALE MOLECULAR POLARITONS

The interaction between plasmonic NPs and molecules is modeled using TDDFT.[46] Due to the relatively large number of considered electrons, we utilize the real-time TDDFT (RT-TDDFT) approach, which is selected because of its superior scaling for large numbers of electrons in comparison to the Casida approach. In this approach, the ground state electron density is perturbed by a weak, spatially uniform electric field (the δ-kick technique[47]) within the dipole approximation and the temporal evolution of the electronic density is recorded. Subsequently, the time dependence of the dipole moment is Fourier-transformed to obtain the photoabsorption spectrum $S(\omega)$ of the system:

$$S^{\nu}(\omega) = \frac{2\omega}{\pi}\,\mathrm{Im}[\mathcal{F}(d^{\nu}(t))] \tag{1}$$

where $\mathcal{F}[d^{\nu}(t)]$ is the Fourier-transformed ν-coordinate of the time-dependent dipole moment $\mathbf{d}(t)$.

The analysis is further extended in terms of transitions between individual Kohn−Sham (KS) states which contribute to photoabsorption:[48]

$$S^{\nu}_{ia}(\omega) = -\frac{4\omega}{\pi}\,\mathrm{Im}[\mu^{\nu *}_{ia}\delta\rho^{\nu}_{ia}(\omega)] \tag{2}$$

where i and a indices numerate occupied and unoccupied KS states, respectively, μ_{ia} is the dipole moment of the $i \rightarrow a$ transition, and $\delta\rho_{ia}(\omega)$ is the Fourier-transformed KS density matrix. The KS decomposition offers insights into the individual single-electron transitions occurring in the system and their associated wave functions, which constitute the *microscopic* perspective.

Simultaneously, it is insightful to investigate the properties (e.g., photoabsorption) of interacting systems from a *macroscopic* point of view utilizing simplified models. Often used is the coupled oscillator model,[1] which recasts potentially complex interactions standing behind the interacting elements as a number of coupled harmonic oscillators. Under the assumption that the driving force of the molecular oscillator is negligible, the photoabsorption spectrum of the system can be expressed as[22]

$$S(\omega) \propto \omega\,\mathrm{Im}\left[\frac{L_{\mathrm{mol}}(\omega)}{L_{\mathrm{mol}}(\omega)L_{\mathrm{pl}}(\omega) - 4g^2\omega^2}\right] \tag{3}$$

where $L_x(\omega) = \omega_x^2 - (\omega + i\gamma_x/2)^2$ are the denominators of Lorentzian-like functions corresponding to the molecular (x = mol) and the plasmonic (x = pl) oscillators, and ω_x and γ_x are, respectively, the resonant energy and width. The coupling strength between the oscillators is g. Because the molecular

https://doi.org/10.1021/acs.jpcc.4c02200
J. Phys. Chem. C XXXX, XXX, XXX−XXX

oscillator is assumed to be driven only by the coupling with the plasmonic oscillator, in the limit of $g \to 0$, the molecular contribution to the absorption vanishes. By definition, the model treats the NP and the molecule uniformly; i.e., all the electronic transitions in an object are unified into a single oscillator. Nevertheless, this approach is ubiquitous in the analysis of experimental and numerical results obtained at different levels of theory,[14,22] allowing a facile estimation of the coupling strength and an intuitive picture of the modifications of the system. Indeed, analysis even at such relatively simple, classical levels can yield fundamental insights into critical aspects of polaritonic systems under various conditions.[49] Hence, our aim in this work is to bridge the two perspectives and pinpoint the atomistic effects that contribute to the observed modifications of the effective properties of the coupled system.

Here, we study a model system consisting of a plasmonic NP and an organic molecule whose resonances are tuned to overlap with each other spectrally to facilitate an efficient interaction. The nanoparticle is a hexagonal magnesium nanoplatelet of approximately 250 atoms and supports a strong LSPR at 4.48 eV. Its molecular counterpart is tetracene whose electronic transition of 4.36 eV matches well the LSPR of the Mg NP (Figure 1a). The two elements are placed in a linear manner, reminiscent of J-aggregates, with the long axis of the molecule along the applied electric field kick (see the inset in Figure 1a). The NP−molecule systems studied here are modeled using the RT-TDDFT method as implemented in the GPAW package[50−52] with a total simulation time of 30 fs, a time step δt = 15 as, and the Perdew−Burke−Ernzerhof (PBE)[53] exchange−correlation functional.

RESULTS AND DISCUSSION

Photoabsorption spectra of the coupled system (Figure 1a) show two clear peaks separated by the so-called Rabi splitting, which increases as the molecule and NP are brought closer together. This behavior is indicative of the formation of two polaritonic branches, the lower polariton (LP) and the upper polariton (UP), and is a characteristic feature of a system in a strong coupling regime. Interestingly, one can observe a gradual widening, a decreasing amplitude, and a red shift of the LP with a shrinking gap. Conversely, UP exhibits only a small blue shift. We analyze this behavior at the *macroscopic* level by fitting the coupled oscillator model to the absorption spectra in Figure 1a. The fitted parameters (Figure 1b,c) indicate that the resonance energies of both oscillators are modified when changing the separation distance; i.e., a change in coupling strength alone is not enough to explain the spectra. The changes are especially large for tetracene. When the molecule approaches the NP, its resonance energy is lowered, reaching 4.18 eV at a gap of 2 Å, an approximately 300 meV red shift versus the isolated molecule. Simultaneously, the fitted width demonstrates a significant increase of the oscillator width, exceeding even the line width of the plasmonic NP at a gap of 2 Å. On the contrary, the NP resonance exhibits a smaller red shift, which additionally appears to be arrested at small gaps. It is noteworthy that for the largest gaps, when $g \to 0$, the molecular resonance is no longer *driven* and cannot be directly detected with the coupled oscillator model in use; it approaches an energy slightly higher than the resonance of the isolated tetracene. Simultaneously, for large gaps, the plasmonic oscillator approaches the resonance of the isolated NP. Overall, the observed oscillator changes are at odds with the commonly used models (e.g., Jaynes−Cummings, Hopfield) in which the new polaritonic modes are composed of unaltered, original eigenmodes. Hence, in the following, we utilize the microscopic analysis to substantiate this apparent inconsistency.

Impact of Kohn−Sham State Hybridization on Photoabsorption. To explain the modifications the system undergoes at small gaps, we turn to the microscopic model and begin the analysis with the atom-projected density of states (pDOS). The nanoparticle/molecular weight is assigned based on the Voronoi decomposition of atomic orbitals with which a given state is expressed on the simulation grid, i.e., the wave functions are divided into the atoms of the NP and the molecule with weights w_{NP} and w_{mol}, respectively, such that $w_{NP} + w_{mol} = 1$ for each state. For better visibility, we select only states with at least a 1% molecular contribution to filter out the numerous Mg states that do not interact with the molecule. As can be seen in Figure 2a, the plotted states, which initially for large gaps are purely molecular, extend to Mg atoms when the gap decreases. This effect is much stronger for the more weakly bound and spatially more extended lowest unoccupied molecular orbital (LUMO) states above the Fermi level of the molecule, which is in agreement with recent findings.[54] In contrast, the initially molecular highest occupied

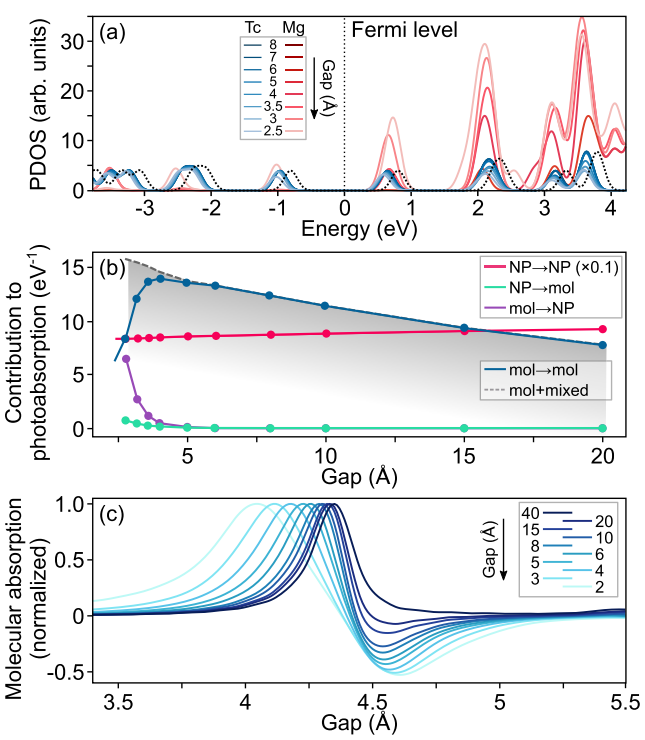

Figure 2. (a) Atom-projected density of states (DOS) with minimum 1% molecular contribution showing increasing modification with decreasing gap. Shades of red correspond to projection onto NP atoms, and shades of blue to molecule atoms. The reference DOS of an isolated tetracene molecule is plotted with black dotted lines. The vertical line is the Fermi level of the molecule. (b) Contributions of each type of transitions to the photoabsorption (absolute values) of the system at the lower polariton energy as a function of gap show an enhancement of molecular absorption with decreasing gaps and a significant rise of mixed transitions below 6 Å. (c) Normalized molecular absorption spectrum for varying gaps shows the in- and out-of-phase polaritons as well as their increased separation and broadening for decreasing separation.

https://doi.org/10.1021/acs.jpcc.4c02200
J. Phys. Chem. C XXXX, XXX, XXX−XXX

molecular orbital (HOMO) states remain confined to the molecule, even for small gaps. Hence, charge transfer can occur when a molecule is excited and electrons instead of occupying a higher molecular energy level transfer to the NP. This tendency is elucidated by an analysis of the different types of Kohn−Sham transitions in the coupled system. We divide them into purely molecular (mol → mol), purely metallic (NP → NP), or mixed originating from or transferring to the molecule (mol → NP, NP → mol, respectively). For this division, see Figure 2b, here presented at the peak of the lower polariton, where the division utilizes the previously introduced NP/molecular weights. The contribution to photoabsorption from each transition (see eq 2) is multiplied by the corresponding weights, e.g., for NP → mol type, the multiplication term is $w^{i}_{NP} \cdot w^{a}_{mol}$, and the absolute value is used.

The dominant contributions to photoabsorption, irrespective of the gap, are transitions occurring in the NP since it contains about six times as many electrons as the molecule. However, as the separation decreases, absorption in the molecule becomes enhanced by nearly a factor of 2 when moving from a 20 to a 5 Å gap. For even smaller gaps, a sudden drop in the molecular absorption is observed with a simultaneous emergence of mixed transitions with the mol → NP ones being dominant, as indicated by the pDOS. The observed quenching of electron generation in tetracene is characteristic of many systems with molecules in close proximity to plasmonic NPs, such as the fluorescence quenching observed in Raman spectroscopy.[55] Here, we directly show how the energy transfer between the molecule and the NP, as evidenced by the mixed transitions, contributes to molecular absorption quenching, even though the sum of all transitions involving the molecule increases monotonically with a diminishing gap (Figure 2b).

Changes of purely molecular absorption caused by a varying gap are seen in detail in the full spectra plotted in Figure 2c. When the molecule is brought closer to the NP, broadening of the molecular absorption is observed, which is in agreement with broadening of the molecular oscillator given by the macroscopic coupled oscillator model. Additionally, a negative contribution to absorption at energies corresponding to the upper polaritonic branch develops, being in line with the formation of an antisymmetric dipole arrangement. On the contrary, at the lower polariton, a symmetric dipole arrangement is observed with positive molecular absorption. Negative photoabsorption can be observed already for the 20 Å gap, which would suggest that strong coupling is already present for such large distances. However, when applying the commonly used criterion for reaching the strong coupling regime, i.e., $g > \sqrt{\gamma_{mol}\gamma_{pl}}$,[22] to the coupled oscillators fit, it is satisfied only for gaps ≤6 Å. The threshold is, however, partially dependent on the arbitrary choice of the broadening parameter used in obtaining the photoabsorption spectrum. This is an evident limitation of TDDFT calculations in which line width broadening for molecules is applied in postprocessing and thereby does not directly affect the coupling mechanisms.

Furthermore, partial photoabsorption spectra (Figure 3a) show that most of the NP, molecular, and mixed absorptions occur around both polaritons. The phase change at the UP is visible not only for molecular absorption but also for the prominent mixed mol → NP transitions. This, combined with the pDOS, suggests that it is mainly the molecular transitions that turn into the mixed mol → NP ones due to hybridization

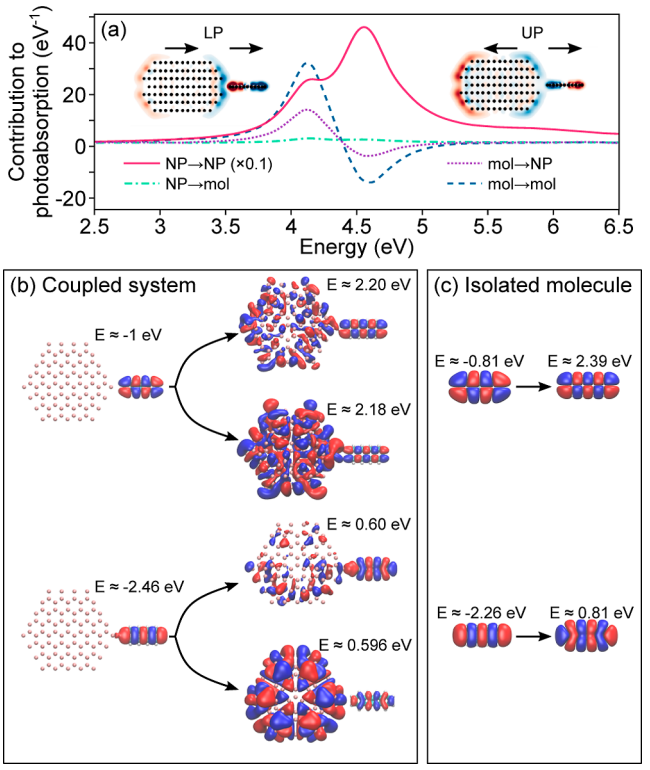

Figure 3. (a) Contributions of each type of transition to the total photoabsorption of the system with a 3 Å gap. The NP → NP contributions are multiplied by 0.1 for better visibility. Insets show the induced electron density at LP and UP energies. The decomposed spectrum sums to the full one. (b) Wave functions of the Kohn−Sham transitions between mixed states active in the strongly coupled system selected for a gap of 3 Å. The energies are given with reference to the Fermi level of the coupled system. (c) Wave functions of the states taking part in the two strongest transitions in the isolated tetracene molecule for reference. The energies are given with respect to the Fermi level of the tetracene molecule.

of the excited states. In contrast, the NP → mol transitions remain in phase with the intra-NP ones but are overall much weaker. The insets in Figure 3a depict the induced electron density for both polaritons, demonstrating the switch to an asymmetric dipole configuration caused by inverting the phase of the molecular transitions at the UP. The gradual shift from mol → mol to mol → NP transitions that occurs below 5 Å means that the LUMO and LUMO + 1 states of tetracene get less populated as the gap decreases, contrary to the regime between 5 and 20 Å where they get more populated with decreasing gap. At the same time, the HOMO and HOMO − 1 states become increasingly depopulated with decreasing gap in the entire range. In the broader context of polaritonically modified chemistry, we would expect chemical transformations that rely on the population of LUMO-states to exhibit a maximum activity around gaps of 5 Å, while transformations relying on the depopulation of the HOMO-states should keep increasing with decreasing gap.

Selected wave functions of initial and final states involved in the optically active mixed mol → NP transitions are plotted in Figure 3b. The transitions in the coupled system resemble those of the isolated molecule (Figure 3c), especially in the molecular parts with the initial wave functions being practically identical. However, the excited states are distributed over the whole system, including the furthest parts of the NP; this again

https://doi.org/10.1021/acs.jpcc.4c02200
J. Phys. Chem. C XXXX, XXX, XXX−XXX

shows the hybridized light−matter nature of the strongly coupled polaritonic states. Such a spatial extension of the final states of the *molecular* transition over the metal NP is also consistent with the red shift of the molecular resonance energy given by the coupled harmonic oscillator. Interestingly, while there are, in principle, multiple/many transitions that contribute to absorption from/to the molecule, the majority of the strength is contributed by only a few KS transitions. Qualitatively, it leads to a lengthening of the dipole resulting in a red shift, as is typically observed when elongating metal NPs, molecules (e.g., benzene, naphthalene, ...), or more generally J-aggregates. A smaller gap causes greater hybridization of the final *molecular* states and ultimately leads to a very strong red shift of what in the *macroscopic* coupled harmonic oscillator model is referred to as the molecular resonance energy ω_{mol} and is plotted in Figure 1b.

Properties of the Plasmonic Nanoresonator. Up to this point, we have focused mainly on modifications of the molecular part. Due to the size difference, it is expected to experience more pronounced changes than its plasmonic counterpart. The NP modes are, however, not indifferent to the presence of the molecule either. Specifically, the electrons present in the molecule screen the plasmon resonance, which is commonly exploited in plasmon-based biosensors[56−58] and is measured as a red shift of the LSPR (Figure 1b). The dipolar contribution to the screened plasmon resonance energy ω_{pl} can be expressed as

$$\omega_{pl}(r) = \omega_{Mg} - a/r^3 \tag{4}$$

where ω_{Mg} is the resonance energy of an isolated Mg NP, a is the screening coefficient, and r is the distance between the interacting dipoles. In the case of the systems studied here, r = gap + Δx = gap + $(x_{mol} + x_{NP})/2$, where x_{mol} and x_{NP} denote the lengths (in the x-direction) of the molecule and the NP, respectively. The screening effect is visible after fitting a coupled oscillator model to the photoabsorption spectra, which allows for extraction of the screening coefficient. For screening by one tetracene (Tc), we obtain $\Delta E_{Tc} = a_{Tc}/\Delta x^3 \approx 0.14$ eV, the theoretical energy shift of the plasmon resonance for a vanishing gap. However, the results in Figure 1b show a plateau for gaps smaller than 3 Å, which can be attributed to interactions between the surface atoms of the NP and the nearby atoms of the molecule.

Moreover, even though the plasmon resonance is a coherent collective response of electrons in the NP, especially for small NPs, such as the one studied here consisting of about 250 atoms, the atomic structure of the object affects the distribution of the electric field in its vicinity. To assess the influence of the inhomogeneous structure of the plasmonic NP on the vacuum electric field E_{vac} experienced by the molecule, and consequently the coupling strength $g = d_{mol}E_{vac}$ (where d_{mol} is the transition dipole moment of the molecule), we evaluate the quasinormal mode (QNM) of the NP. To that end, we replace the NP with an ellipsoidal Mg nanoresonator of matching dimensions and an effective Drude permittivity function which together match the TDDFT-calculated photoabsorption spectrum. Next, we perform a classical electromagnetic calculation to find the complex eigenfrequencies of the QNMs and obtain the QNM field distribution at the LSPR.[59] Finally, we evaluate the interaction of a point dipole at the position of the molecule with the QNM to obtain the mode volume V_{QNM} and the resulting expected coupling strength g_{QNM}

$$g_{QNM} = d_{mol}E_{vac}^{QNM} = d_{mol}\sqrt{\frac{h\nu_{QNM}}{2\epsilon\epsilon_0 V_{QNM}}} \tag{5}$$

Here, h denotes the Planck constant, ϵ and ϵ_0 are the permittivities of the surrounding medium and vacuum, respectively, and ν_{QNM} is the QNM eigenfrequency. As seen in Figure 4a, the coupling strength obtained from fitting the

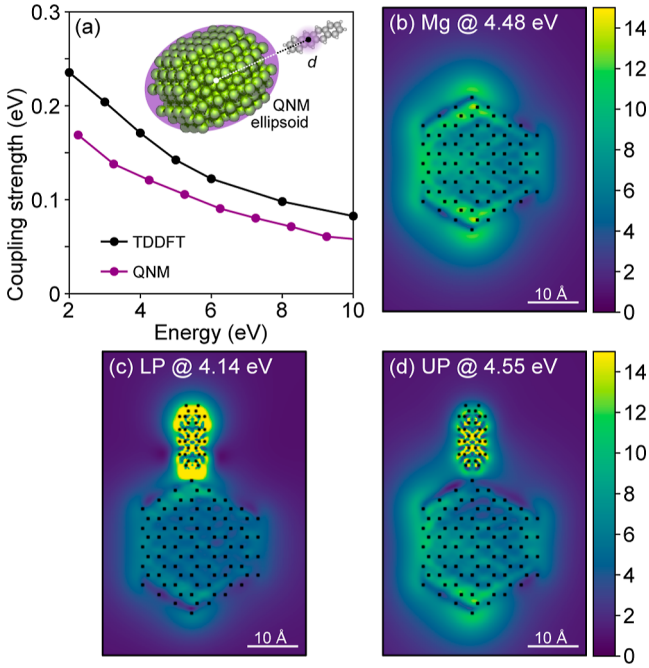

Figure 4. (a) The coupling strength obtained from quasinormal mode (QNM) predictions and TDDFT calculations fitted with the coupled oscillator model as a function of NP−molecule gap. The point-dipole used in QNM calculations is placed at ≈40% of the molecule length (see the inset for schematic illustration) to account for the decay of the electric field of the plasmon. (b) Electromagnetic field enhancement in an isolated Mg NP at the plasmon resonance. (c,d) Electromagnetic field enhancement in the strongly coupled system of Mg NP and tetracene for 3 Å gap at the (c) lower and (d) upper polaritons.

TDDFT photoabsorption exceeds the QNM predictions. The induced electric field at the plasmon resonance energy exhibits clear hot spots near the molecule position (Figure 4b) as the vertices protruding toward the molecule result in locally higher values of the vacuum electric field experienced by the molecule, effectively increasing the coupling strength. Simultaneously, the molecule itself modifies the decaying electric field by localizing it within its volume. At both polaritons in a strongly coupled system, on the other hand, the electric field is enhanced in the gap between the NP and the molecule and in the molecule itself (Figure 4c,d).

Impact of Moiety Number and Type on System Coupling. The geometry of the system influences the coupling and the degree of modification of the properties of both the NP and the molecule. We compare the initial system (gap 3 Å) with two new ones (identical NP−mol gap): one consisting of a Mg NP and two tetracene molecules and the second consisting of two NP and a single tetracene molecule

https://doi.org/10.1021/acs.jpcc.4c02200
J. Phys. Chem. C XXXX, XXX, XXX−XXX

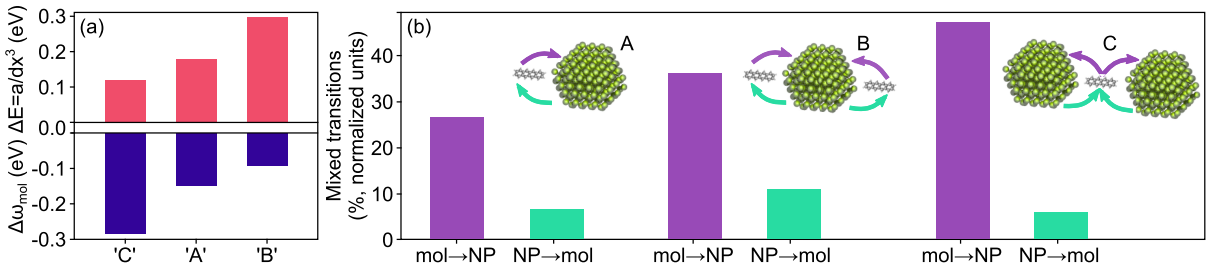

Figure 5. (a) Theoretical plasmon resonance energy shift for gap = 0: $\Delta E = a/dx^3$ for three geometries in question (up) and the shift of molecular oscillator resonance energy (down) obtained from the coupled oscillators model. (b) Summed contribution of mixed transitions in the coupled system with a gap of 3 Å for various geometries. The contribution is normalized with respect to the total photoabsorption of the system. The inset shows the investigated geometries.

(see the inset in Figure 5). In general, modifications of the plasmonic oscillator are larger when the ratio of molecules per NP increases. Namely, the additional tetracene increases ΔE_{pl} (the screening), whereas adding another NP decreases ΔE_{pl}, where both shifts are relative to the system without the molecule(s). Similarly, an additional NP results in a larger $\Delta\omega_{mol}$ and an additional tetracene molecule decreases $\Delta\omega_{mol}$ (Figure 5a). However, the above trade-offs in the relative plasmon and molecule resonance shifts do not transfer when analyzing coupling between the Kohn−Sham states of the systems. Specifically, for mol → NP transitions, an additional molecule or a NP increases the possibility of hybridization between electronic states owing to a large density of states in the NP. Consequently, this yields a larger contribution of mol → NP transitions. On the other hand, more NP → mol transitions are observed only for the case with two tetracene molecules. Due to a limited amount of available molecular states (as compared to the NP), the tetracene molecule is the limiting factor and hybridization of the electronic states between a NP dimer and one molecule gives the same contribution of NP → mol mixed transitions to photoabsorption as for a single NP coupled to one tetracene molecule.

As an alternative avenue to extend our understanding of the role of strong coupling in the observed phenomena, we extend our analysis to systems that incorporate molecules expected to exhibit weak coupling with the Mg NP. Replacing tetracene with a different molecule or adding another molecule to the system enables a quantitative comparison of the systems and presents a more realistic instance in which strong and weak couplings are simultaneously present. The molecule of choice is naphthalene, which supports an electronic transition at 5.9 eV that is detuned from the LSPR of the Mg NP and has a dipole moment smaller than that of tetracene. However, it simultaneously has an atomic structure similar to that of tetracene, which allows for a nearly invariant atomistic environment in the immediate vicinity of the NP−molecule gap.

In the Mg NP−naphthalene system, Rabi splitting is not observed, but the presence of the molecule is manifested in the red shift of the photoabsorption spectrum of the LSPR (Figure 6a). When naphthalene is added to the strongly coupled Mg NP−tetracene system, Rabi splitting is still visible, but the UP branch is red-shifted due to screening. Equation 4 can be rewritten in the case of two different screening molecules as

$$\omega_{pl}(r) = \omega_{Mg} - (a_{Ntl}/r_{Ntl}^3 + a_{Tc}/r_{Tc}^3) \quad (6)$$

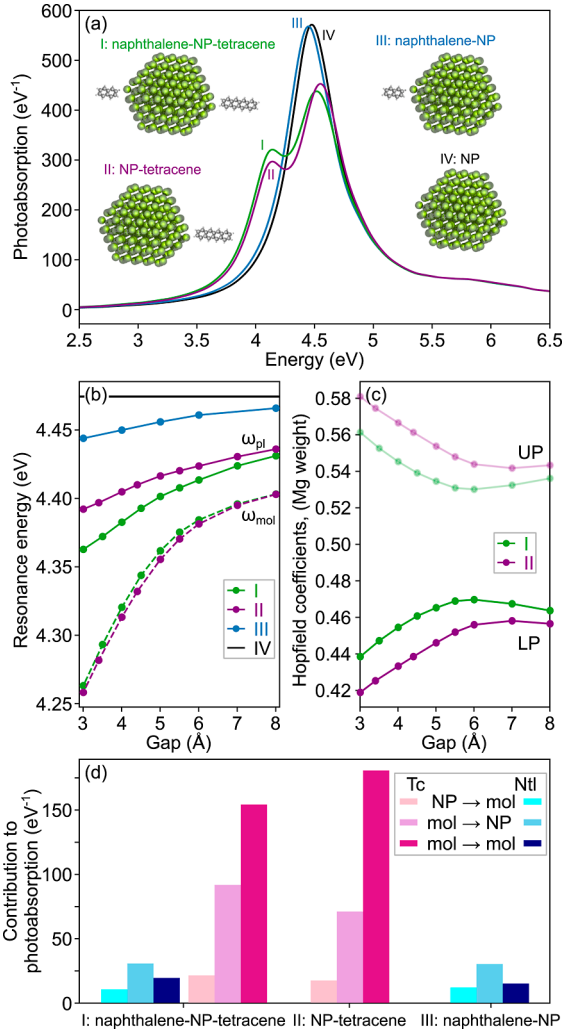

Figure 6. (a) Photoabsorption spectra in (I) the naphthalene−Mg NP−tetracene, (II) Mg NP−tetracene, (III) Mg NP−naphthalene, and (IV) isolated Mg NP systems for a gap of 3 Å. (b) Fitted resonance energies of the oscillators in systems I−IV. (c) Hopfield mixing coefficients of the Mg moiety for polaritonic branches in systems I and II. (d) Photoabsorption related to mixed and molecular transitions in systems I−III for a gap of 3 Å summed over 3−6.5 eV energy range.

where the subscripts Tc and Ntl denote, respectively, tetracene and naphthalene. By fitting the above, we obtain $\Delta E_{Tc-Ntl} \approx$ 0.18 eV, which is approximately the sum of the individual red shifts of the NP−tetracene and NP−naphthalene systems

https://doi.org/10.1021/acs.jpcc.4c02200
J. Phys. Chem. C XXXX, XXX, XXX−XXX

($\Delta E_{Tc} \approx 0.14$ eV and $\Delta E_{Ntl} \approx 0.05$ eV, respectively). Irrespective of the plasmon shift, the fitted molecular oscillator resonance remains similar for both systems (Figure 6b).

Another modification introduced by naphthalene is the change in the relative amplitudes of the polaritons, visible in the photoabsorption spectrum and manifested in the Hopfield mixing coefficients (Figure 6c), which for the NP−tetracene case (system II) show a slightly unequal contribution of the Mg and molecular moieties to both polaritons. As expected, the additional presence of naphthalene increases the level of screening experienced by the Mg NP. Interestingly, the resulting red shift of the plasmon and thus the smaller detuning between the NP cavity and tetracene cause greater light−matter mixing of the two moieties in both polaritonic branches. However, this does not affect the coupling strength. This increased mixing is also visible at the level of single Kohn−Sham transitions, manifesting in greater contributions of mixed transitions to photoabsorption (Figure 6d). Transitions involving naphthalene (i.e., Ntl → Ntl, Ntl → NP, and NP → Ntl) are of almost identical intensity in both the Mg NP−naphthalene and naphthalene−Mg NP−tetracene systems (here separated by a gap of 3 Å). Transitions involving tetracene, however, are modified by the presence of naphthalene. Specifically, adding naphthalene to the Mg NP−tetracene system increases the magnitude of contributions of mixed tetracene/NP transitions (especially for tetracene → NP transitions) and simultaneously lowers the contribution of purely molecular intratetracene transitions.

Finally, we divide the molecular absorption in the naphthalene−Mg NP−tetracene system into contributions from molecules of both types (Figure 7a). The main difference between tetracene and naphthalene is that the strongly coupled tetracene molecule experiences much more absorption enhancement when it is brought closer to the NP than the weakly coupled naphthalene molecule. Analogously to the Mg NP−tetracene system studied initially, absorption quenching is observed for small gaps (≤4 Å). By accounting for both transitions to and from the molecule, monotonous growth of the absorption with a diminishing gap is observed. However, in comparison to that of tetracene, the naphthalene enhancement is approximately 10 times smaller. The much smaller absorption enhancement in the weakly coupled molecule means that the mixed transitions, being the result of molecular Kohn−Sham transitions coupling to NP ones, will as a consequence not have a significant contribution to the photoabsorption but are in principle present for small gaps. Differences between the naphthalene and the tetracene interactions with the NP are also seen in the electric field enhancement in the system (Figure 7b). Most of the field is focused near the tetracene molecule, especially on the gap side. Naphthalene lacks such *focusing*, and there is no significant enhancement in the induced field in its surrounding, irrespective of the considered energy.

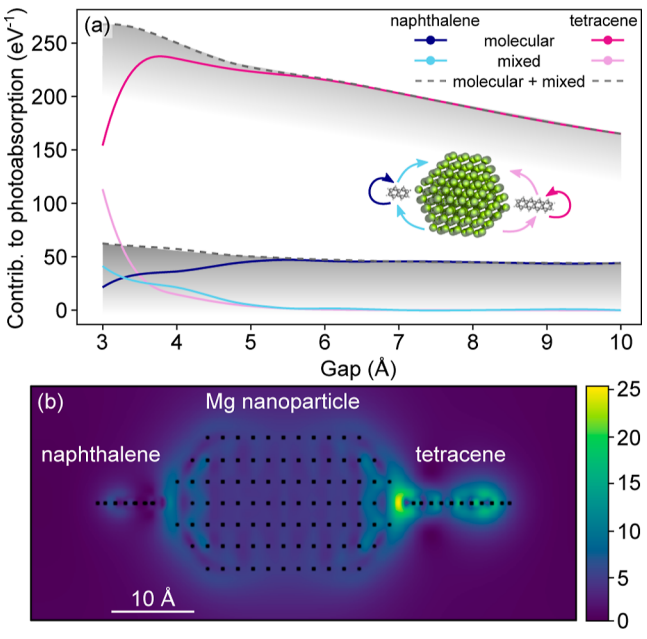

Figure 7. (a) Photoabsorption related to mixed and molecular transitions in the naphthalene−Mg NP−tetracene system for a gap of 3 Å, summed over 3−6.5 eV energy range. (b) Electric field enhancement in the naphthalene−Mg NP−tetracene system for a gap of 3 Å at the LP energy, i.e., 3.90 eV; side view. There is a hot spot visible between the Mg NP and tetracene.

CONCLUSIONS

Through a TDDFT investigation of a system composed of a metallic particle nanocavity and an organic molecule, we elucidate the relations between the macroscopic and microscopic observables used to describe effects occurring during the transition from weak to strong light−matter interactions. The macroscopic description, centered around the ubiquitously used coupled harmonic oscillator-based model, determines the physical changes in the system for a decreasing gap as a predictable increase of the coupling strength, which is accompanied by nontrivial modifications of the parameters of the constituent elements. Specifically, the effective resonance positions and widths of the plasmon and molecule change with the separation distance. These changes, namely the red shifts of both resonances and the increasing width of the molecular transition are tied to *microscopic* changes of the electronic density and evolution of hybridized plasmon-molecule Kohn−Sham states.

We find that the cause of the increase of the molecular line width, which is inversely proportional to the gap size, is the increased mixing of the nominal molecular KS states with those of the Mg NP. At the *microscopic* level, such mixing increases the decoherence probability of the excited states into single electron−hole pairs, which is visible in the increased mixed transitions and leads to a *macroscopic* increase of γ_{mol}. Simultaneously, the molecular transition exhibits a significant red shift from about 4.4 eV at a gap size of 6 Å to less than 4.2 eV for smaller gaps. This effect is likewise connected to the rise of hybridized KS states and the emergence of mixed transitions at a gap of 6 Å. The excited *molecular* KS states acquire an increasing magnesium contribution which causes a spatial enlargement of the dipolar transition and a concomitant red shift. This effect can be thought of as an analogue of a plasmonic red shift due to the elongation of a metal NP or alternatively J-aggregate stacking. Finally, the magnesium NP red shift is caused by electrostatic screening by the "body of the molecule", i.e., the remaining electrons involved in higher energy KS transitions in the molecule. At very small gaps, the red shift is slightly arrested by partial charge transfer to the NP. These findings offer insights into modifications of the strongly coupled systems and pave the way to deeper understanding of the strong light−matter coupling mechanisms, as well as the possibilities of tailoring the material properties they create.

https://doi.org/10.1021/acs.jpcc.4c02200
J. Phys. Chem. C XXXX, XXX, XXX−XXX

AUTHOR INFORMATION

Corresponding Author

Tomasz J. Antosiewicz − *Faculty of Physics, University of Warsaw, PL-02-093 Warsaw, Poland; Department of Physics, Chalmers University of Technology, SE-412 96 Gothenburg, Sweden;* orcid.org/0000-0003-2535-4174; Email: tomasz.antosiewicz@fuw.edu.pl

Authors

Maria Bancerek − *Faculty of Physics, University of Warsaw, PL-02-093 Warsaw, Poland; Department of Physics, Chalmers University of Technology, SE-412 96 Gothenburg, Sweden*

Jakub Fojt − *Department of Physics, Chalmers University of Technology, SE-412 96 Gothenburg, Sweden*

Paul Erhart − *Department of Physics, Chalmers University of Technology, SE-412 96 Gothenburg, Sweden;* orcid.org/0000-0002-2516-6061

Complete contact information is available at: https://pubs.acs.org/10.1021/acs.jpcc.4c02200

Notes

The authors declare no competing financial interest.

ACKNOWLEDGMENTS

We acknowledge support from the Polish National Science Center via the project 2019/34/E/ST3/00359 and the Knut and Alice Wallenberg Foundation under grant no. 2019.0140. Calculations were made at the Interdisciplinary Centre for Mathematical and Computational Modelling, University of Warsaw, project #G55-6, as well as using resources provided by the Swedish National Infrastructure for Computing (SNIC) at NSC, C3SE, and PDC, partially funded by the Swedish Research Council through grant agreement no. 2018-05973.

REFERENCES

(1) Törmä, P.; Barnes, W. L. Strong coupling between surface plasmon polaritons and emitters: a review. *Rep. Prog. Phys.* **2015**, *78*, 013901.

(2) Garcia-Vidal, F. J.; Ciuti, C.; Ebbesen, T. W. Manipulating matter by strong coupling to vacuum fields. *Science* **2021**, *373*, No. eabd0336.

(3) Baranov, D. G.; Wersäll, M.; Cuadra, J.; Antosiewicz, T. J.; Shegai, T. Novel Nanostructures and Materials for Strong Light−Matter Interactions. *ACS Photonics* **2018**, *5*, 24−42.

(4) Piejko, M.; Patrahau, B.; Joseph, K.; Muller, C.; Devaux, E.; Ebbesen, T. W.; Moran, J. Solvent Polarity under Vibrational Strong Coupling. *J. Am. Chem. Soc.* **2023**, *145*, 13215−13222.

(5) Thomas, A.; Lethuillier-Karl, L.; Nagarajan, K.; Vergauwe, R. M. A.; George, J.; Chervy, T.; Shalabney, A.; Devaux, E.; Genet, C.; Moran, J.; et al. Tilting a ground-state reactivity landscape by vibrational strong coupling. *Science* **2019**, *363*, 615−619.

(6) Orgiu, E.; George, J.; Hutchison, J. A.; Devaux, E.; Dayen, J. F.; Doudin, B.; Stellacci, F.; Genet, C.; Schachenmayer, J.; Genes, C.; et al. Conductivity in organic semiconductors hybridized with the vacuum field. *Nat. Mater.* **2015**, *14*, 1123−1129.

(7) Aroeira, G. J. R.; Kairys, K. T.; Ribeiro, R. F. Coherent transient exciton transport in disordered polaritonic wires. *Nanophotonics* **2024**, *0*, ASAP.

(8) Virgili, T.; Coles, D.; Adawi, A. M.; Clark, C.; Michetti, P.; Rajendran, S. K.; Brida, D.; Polli, D.; Cerullo, G.; Lidzey, D. G. Ultrafast polariton relaxation dynamics in an organic semiconductor microcavity. *Phys. Rev. B: Condens. Matter Mater. Phys.* **2011**, *83*, 245309.

(9) Wang, S.; Chervy, T.; George, J.; Hutchison, J. A.; Genet, C.; Ebbesen, T. W. Quantum Yield of Polariton Emission from Hybrid Light-Matter States. *J. Phys. Chem. Lett.* **2014**, *5*, 1433−1439.

(10) Munkhbat, B.; Wersäll, M.; Baranov, D. G.; Antosiewicz, T. J.; Shegai, T. Suppression of photo-oxidation of organic chromophores by strong coupling to plasmonic nanoantennas. *Sci. Adv.* **2018**, *4*, No. eaas9552.

(11) Nehl, C. L.; Hafner, J. H. Shape-dependent plasmon resonances of gold nanoparticles. *J. Mater. Chem.* **2008**, *18*, 2415−2419.

(12) Bozhevolnyi, S. I.; Khurgin, J. B. The case for quantum plasmonics. *Nat. Photonics* **2017**, *11*, 398−400.

(13) Urbieta, M.; Barbry, M.; Zhang, Y.; Koval, P.; Sánchez-Portal, D.; Zabala, N.; Aizpurua, J. Atomic-Scale Lightning Rod Effect in Plasmonic Picocavities: A Classical View to a Quantum Effect. *ACS Nano* **2018**, *12*, 585−595.

(14) Wu, X.; Gray, S. K.; Pelton, M. Quantum-dot-induced transparency in a nanoscale plasmonic resonator. *Opt. Express* **2010**, *18*, 23633−23645.

(15) Zengin, G.; Wersäll, M.; Nilsson, S.; Antosiewicz, T. J.; Käll, M.; Shegai, T. Realizing Strong Light-Matter Interactions between Single-Nanoparticle Plasmons and Molecular Excitons at Ambient Conditions. *Phys. Rev. Lett.* **2015**, *114*, 157401.

(16) Sugawara, Y.; Kelf, T. A.; Baumberg, J. J.; Abdelsalam, M. E.; Bartlett, P. N. Strong Coupling between Localized Plasmons and Organic Excitons in Metal Nanovoids. *Phys. Rev. Lett.* **2006**, *97*, 266808.

(17) Wang, H.; Toma, A.; Wang, H.-Y.; Bozzola, A.; Miele, E.; Haddadpour, A.; Veronis, G.; De Angelis, F.; Wang, L.; Chen, Q.-D.; et al. The role of Rabi splitting tuning in the dynamics of strongly coupled J-aggregates and surface plasmon polaritons in nanohole arrays. *Nanoscale* **2016**, *8*, 13445−13453.

(18) Schlather, A. E.; Large, N.; Urban, A. S.; Nordlander, P.; Halas, N. J. Near-Field Mediated Plexcitonic Coupling and Giant Rabi Splitting in Individual Metallic Dimers. *Nano Lett.* **2013**, *13*, 3281−3286.

(19) Santhosh, K.; Bitton, O.; Chuntonov, L.; Haran, G. Vacuum Rabi splitting in a plasmonic cavity at the single quantum emitter limit. *Nat. Commun.* **2016**, *7*, 11823.

(20) Chikkaraddy, R.; de Nijs, B.; Benz, F.; Barrow, S. J.; Scherman, O. A.; Rosta, E.; Demetriadou, A.; Fox, P.; Hess, O.; Baumberg, J. J. Single-molecule strong coupling at room temperature in plasmonic nanocavities. *Nature* **2016**, *535*, 127−130.

(21) Groß, H.; Hamm, J. M.; Tufarelli, T.; Hess, O.; Hecht, B. Near-field strong coupling of single quantum dots. *Sci. Adv.* **2018**, *4*, No. eaar4906.

(22) Rossi, T. P.; Shegai, T.; Erhart, P.; Antosiewicz, T. J. Strong plasmon-molecule coupling at the nanoscale revealed by first-principles modeling. *Nat. Commun.* **2019**, *10*, 3336.

(23) Kuisma, M.; Rousseaux, B.; Czajkowski, K. M.; Rossi, T. P.; Shegai, T.; Erhart, P.; Antosiewicz, T. J. Ultrastrong Coupling of a Single Molecule to a Plasmonic Nanocavity: A First-Principles Study. *ACS Photonics* **2022**, *9*, 1065−1077.

(24) Ruggenthaler, M.; Sidler, D.; Rubio, A. Understanding Polaritonic Chemistry from Ab Initio Quantum Electrodynamics. *Chem. Rev.* **2023**, *123*, 11191−11229.

(25) Ye, H.; Becca, J. C.; Jensen, L. Modeling the near-field effect on molecular excited states using the discrete interaction model/quantum mechanical method. *J. Chemn. Phys.* **2024**, *160*, 014707.

(26) Mokkath, J. H. Interface plasmon damping in the $Cd_{33}Se_{33}$/Ti_2C MXene heterostructure. *Phys. Chem. Chem. Phys.* **2023**, *25*, 28761−28769.

(27) Miwa, K.; Sakamoto, S.; Ishizaki, A. Control and Enhancement of Single-Molecule Electroluminescence through Strong Light-Matter Coupling. *Nano Lett.* **2023**, *23*, 3231−3238.

(28) Jamshidi, Z.; Kargar, K.; Mendive-Tapia, D.; Vendrell, O. Coupling Molecular Systems with Plasmonic Nanocavities: A Quantum Dynamics Approach. *J. Phys. Chem. Lett.* **2023**, *14*, 11367−11375.

(29) Dey, A.; Mendalz, A.; Wach, A.; Vadell, R. B.; Silveira, V. R.; Leidinger, P. M.; Huthwelker, T.; Shtender, V.; Novotny, Z.; Artiglia, L.; et al. Hydrogen evolution with hot electrons on a plasmonic-molecular catalyst hybrid system. *Nat. Commun.* **2024**, *15*, 445.
(30) Hutchison, J. A.; Schwartz, T.; Genet, C.; Devaux, E.; Ebbesen, T. W. Modifying Chemical Landscapes by Coupling to Vacuum Fields. *Angew. Chem., Int. Ed.* **2012**, *51*, 1592−1596.
(31) Thomas, A.; George, J.; Shalabney, A.; Dryzhakov, M.; Varma, S. J.; Moran, J.; Chervy, T.; Zhong, X.; Devaux, E.; Genet, C.; et al. Ground-State Chemical Reactivity under Vibrational Coupling to the Vacuum Electromagnetic Field. *Angew. Chem., Int. Ed.* **2016**, *55*, 11462−11466.
(32) de Nijs, B.; Benz, F.; Barrow, S. J.; Sigle, D. O.; Chikkaraddy, R.; Palma, A.; Carnegie, C.; Kamp, M.; Sundararaman, R.; Narang, P.; et al. Plasmonic tunnel junctions for single-molecule redox chemistry. *Nat. Commun.* **2017**, *8*, 994.
(33) Zhang, Z.; Zhang, C.; Zheng, H.; Xu, H. Plasmon-Driven Catalysis on Molecules and Nanomaterials. *Acc. Chem. Res.* **2019**, *52*, 2506−2515.
(34) Wang, X.; Mao, Y.; Wang, Z. Plasmonic-assisted Electrocatalysis for CO2 Reduction Reaction. *ChemElectroChem* **2024**, *11*, No. e202300805.
(35) George, J.; Singh, J. Polaritonic Chemistry: Band-Selective Control of Chemical Reactions by Vibrational Strong Coupling. *ACS Catal.* **2023**, *13*, 2631−2636.
(36) Andrews, D. L.; Bradshaw, D. S.; Dinshaw, R.; Scholes, G. D. *Photonics: Biomedical Photonics, Spectroscopy, and Microscopy*; Andrews, D. L., Ed.; John Wiley & Sons, Inc.: Hoboken, NJ, 2015; pp 101−127.
(37) Kluczyk-Korch, K.; Antosiewicz, T. J. Hot carrier generation in a strongly coupled molecule−plasmonic nanoparticle system. *Nanophotonics* **2023**, *12*, 1711−1722.
(38) Chen, D.; Zhang, Y.; Meng, S. Molecular Orbital Insights into Plasmon-Induced Methane Photolysis. *Nano Lett.* **2023**, *23*, 11638−11644.
(39) Kumar, P. V.; Rossi, T. P.; Marti-Dafcik, D.; Reichmuth, D.; Kuisma, M.; Erhart, P.; Puska, M. J.; Norris, D. J. Plasmon-Induced Direct Hot-Carrier Transfer at Metal−Acceptor Interfaces. *ACS Nano* **2019**, *13*, 3188−3195.
(40) Fojt, J.; Rossi, T. P.; Kuisma, M.; Erhart, P. Hot-Carrier Transfer across a Nanoparticle−Molecule Junction: The Importance of Orbital Hybridization and Level Alignment. *Nano Lett.* **2022**, *22*, 8786−8792.
(41) Cascino, L.; Corni, S.; D'Agostino, S. Revealing the Interplay between Hybrid and Charge-Transfer States in Polariton Chemistry. *J. Phys. Chem. C* **2024**, *128*, 2917−2927.
(42) Schäfer, C.; Ruggenthaler, M.; Appel, H.; Rubio, A. Modification of excitation and charge transfer in cavity quantum-electrodynamical chemistry. *Proc. Natl. Acad. Sci. U.S.A.* **2019**, *116*, 4883−4893.
(43) Sokolovskii, I.; Tichauer, R. H.; Morozov, D.; Feist, J.; Groenhof, G. Multi-scale molecular dynamics simulations of enhanced energy transfer in organic molecules under strong coupling. *Nat. Commun.* **2023**, *14*, 6613.
(44) Li, T. E.; Hammes-Schiffer, S. QM/MM Modeling of Vibrational Polariton Induced Energy Transfer and Chemical Dynamics. *J. Am. Chem. Soc.* **2023**, *145*, 377−384.
(45) Martínez-Martínez, L. A.; Eizner, E.; Kéna-Cohen, S.; Yuen-Zhou, J. Triplet harvesting in the polaritonic regime: A variational polaron approach. *J. Chem. Phys.* **2019**, *151*, 054106.
(46) Runge, E.; Gross, E. K. U. Density-Functional Theory for Time-Dependent Systems. *Phys. Rev. Lett.* **1984**, *52*, 997−1000.
(47) Yabana, K.; Bertsch, G. F. Time-dependent local-density approximation in real time. *Phys. Rev. B: Condens. Matter Mater. Phys.* **1996**, *54*, 4484−4487.
(48) Rossi, T. P.; Kuisma, M.; Puska, M. J.; Nieminen, R. M.; Erhart, P. Kohn-Sham decomposition in real-time time-dependent density-functional theory: An efficient tool for analyzing plasmonic excitations. *J. Chem. Theory Comput.* **2017**, *13*, 4779−4790.
(49) Canales, A.; Karmstrand, T.; Baranov, D. G.; Antosiewicz, T. J.; Shegai, T. O. Polaritonic linewidth asymmetry in the strong and ultrastrong coupling regime. *Nanophotonics* **2023**, *12*, 4073−4086.
(50) Enkovaara, J.; Rostgaard, C.; Mortensen, J.; Chen, J.; Dulak, M.; Ferrighi, L.; Gavnholt, J.; Glinsvad, C.; Haikola, V.; Hansen, H.; Kristoffersen, H.; et al. Electronic structure calculations with GPAW: a real-space implementation of the projector augmented-wave method. *J. Phys.: Condens. Matter* **2010**, *22*, 253202.
(51) Mortensen, J. J.; Larsen, A. H.; Kuisma, M.; Ivanov, A. V.; Taghizadeh, A.; Peterson, A.; Haldar, A.; Dohn, A. O.; Schäfer, C.; Jónsson, E. Ö.; et al. GPAW: An open Python package for electronic structure calculations. *J. Chem. Phys.* **2024**, *160*, 092503.
(52) Kuisma, M.; Sakko, A.; Rossi, T.; Larsen, A.; Enkovaara, J.; Lehtovaara, L.; Rantala, T. Localized surface plasmon resonance in silver nanoparticles: Atomistic first-principles time-dependent density-functional theory calculations. *Phys. Rev. B: Condens. Matter Mater. Phys.* **2015**, *91*, 115431.
(53) Perdew, J. P.; Burke, K.; Ernzerhof, M. Generalized Gradient Approximation Made Simple. *Phys. Rev. Lett.* **1996**, *77*, 3865−3868.
(54) Babaze, A.; Esteban, R.; Borisov, A. G.; Aizpurua, J. Electronic Exciton−Plasmon Coupling in a Nanocavity Beyond the Electromagnetic Interaction Picture. *Nano Lett.* **2021**, *21*, 8466−8473.
(55) Walters, C. M.; Pao, C.; Gagnon, B. P.; Zamecnik, C. R.; Walker, G. C. Bright Surface-Enhanced Raman Scattering with Fluorescence Quenching from Silica Encapsulated J-Aggregate Coated Gold Nanoparticles. *Adv. Mater.* **2018**, *30*, 1705381.
(56) Mejía-Salazar, J. R.; Oliveira, O. N. J. Plasmonic Biosensing. *Chem. Rev.* **2018**, *118*, 10617−10625.
(57) Garoli, D.; Calandrini, E.; Giovannini, G.; Hubarevich, A.; Caligiuri, V.; De Angelis, F. Nanoporous gold metamaterials for high sensitivity plasmonic sensing. *Nanoscale Horiz.* **2019**, *4*, 1153−1157.
(58) Antosiewicz, T. J.; Apell, S. P.; Claudio, V.; Käll, M. A simple model for the resonance shift of localized plasmons due to dielectric particle adhesion. *Opt. Express* **2012**, *20*, 524−533.
(59) Yan, W.; Faggiani, R.; Lalanne, P. Rigorous modal analysis of plasmonic nanoresonators. *Phys. Rev. B* **2018**, *97*, 205422.

https://doi.org/10.1021/acs.jpcc.4c02200
J. Phys. Chem. C XXXX, XXX, XXX−XXX